Contract No:

This document was prepared in conjunction with work accomplished under Contract No. DE-AC09-08SR22470 with the U.S. Department of Energy (DOE) Office of Environmental Management (EM).

Disclaimer:

In-Situ Gamma-Ray Assay of the West Cell Line in the 235-F Plutonium Fuel Form Facility

A.H. Couture – Pajarito Scientific Corporation

D.P. Diprete – Savannah River National Laboratory

September 2014

SRNL-STI-2014-00440 Revision 0

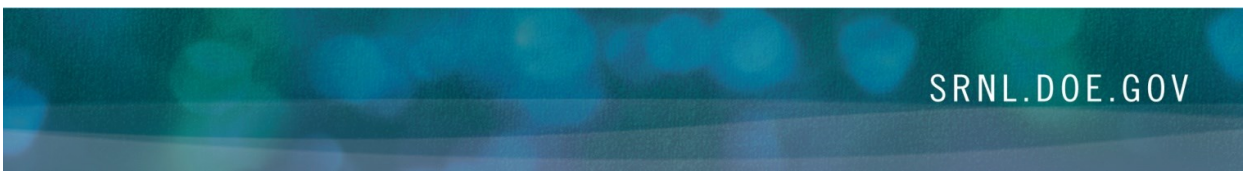

DISCLAIMER

Printed in the United States of America

Prepared for
U.S. Department of Energy

SRNL-STI-2014-00440
Revision 0

Keywords: 235-F, Non-destructive Assay, Heat-Source Plutonium, PuFF

Retention: *Permanent*

In-Situ Gamma-Ray Assay of the West Cell Line in the 235-F Plutonium Fuel Form Facility

A.H. Couture
D.P. Diprete

September 2014

Prepared for the U.S. Department of Energy under contract number DE-AC09-08SR22470.

Savannah River National Laboratory™
OPERATED BY SAVANNAH RIVER NUCLEAR SOLUTIONS

EXECUTIVE SUMMARY

On August 29th, 2013, scientists from SRNL took a series of in-situ gamma-ray measurements in the maintenance trench beneath Cells 6-9 on the west line of the PuFF facility using an uncollimated, high-purity germanium detector. The detector efficiency was estimated using a combination of MCNP simulations and empirical measurements. Data analysis was performed using three gamma-rays emitted by Pu-238 (99.85 keV, 152.7 keV, and 766.4 keV) providing three independent estimates of the mass of Pu-238 holdup in each of the cells. The weighted mean of these three results was used as the best estimate of Pu-238 holdup in the West Cell Line of PuFF. The results of the assay measurements are found in the table below along with the results from the scoping assay performed in 2006 [3]. All uncertainties in this table (as well as the rest of the report) are given as 1σ. The total holdup in the West Cell Line was 2.4 ± 0.7 grams. This result is 0.6 g higher than the previous estimate, a 0.4σ difference.

These results should be considered preliminary since measurements inside the West Cell line are scheduled for Spring of 2015. Those measurements will provide detailed information about the distribution of Pu-238 in the cells to be used to refine the results of the current assay.

Cell	Current Assay Mass (g)	2006 Scoping Assay Mass (g) [3]
6	2.2 ± 0.7 (32%)	1.78 ± 1.21 (68%)
7	0.25 ± 0.08 (30%)	0.055 ± 0.045 (82%)
8	< 0.004	< 0.00784
9	< 0.004	< 0.00911
Total West Cell Line	2.4 ± 0.7 (29%)	1.8 ± 1.2 (66%)

TABLE OF CONTENTS

LIST OF TABLES

LIST OF FIGURES

LIST OF ABBREVIATIONS

cm	centimeter
Bq	Bequerel (decays per second)
FWHM	Full-Width at Half-Maximum
HEPA	High-Efficiency Particulate Air (filter)
HPGe	High-Purity Germanium Detector
keV	kilo-electron-Volt
LaBr	Lanthanum Bromide
LANL	Los Alamos National Laboratory
LN	Liquid nitrogen
MCA	Multi-channel Analyzer
MCNP	Monte-Carlo N-Particle Transport Code
MCNP5	Monte-Carlo N-Particle Transport Code, Version 5
mm	millimeter
NDA	Non-destructive Assay
PuFF	Plutonium Fuel Form Facility
PSC	Pajarito Scientific Corporation
SRNL	Savannah River National Laboratory
SRS	Savannah River Site
WBS	Work Breakdown Structure

1.0 Introduction

The Plutonium Fuel Form (PuFF) facility is located in Building 235-F near the geographic center of the Savannah River Site. The facility was used to produce iridium-encapsulated Pu-238 spheres and pellets for use as radioisotope thermal generators, primarily for the space program. The facility is divided between two cell lines, the east cell line used to process the powdered Pu-238 oxide raw material into fuel forms and the west cell line used to encapsulate the fuel forms in iridium. Between 1978 and 1984, the PuFF facility processed approximately 165 kilograms of Pu-238. In 1984, the facility was placed in "enhanced readiness mode", which consisted of reducing staff to the minimum required to keep the facility maintained in operating condition while waiting for a new mission. During this time, the inert argon atmosphere in the east cell line was not maintained. The purpose of the inert argon atmosphere was to prevent corrosion from the high-alpha activity of Pu-238. Corrosion soon made the east cell line inoperable, particularly the aluminum remote manipulators. The facility has not been decontaminated since the intent was to continue operations and after the failure of the manipulators much of the facility is inaccessible [1].

Scoping in-situ gamma-ray assays were performed in the PuFF facility in 2006 [3]. The current estimate of Pu-238 holdup in the facility is based upon these measurements. Using this holdup estimate as a source term, SRS has performed a risk analysis that indicated a seismic event that induces a full-facility fire in 235-F could lead to a 28,800 rem dose to a co-located worker [7]. Based on this risk assessment, SRS is taking steps to decontaminate the facility. One of the first steps taken is to improve upon the quality of the in-situ gamma-ray assay data. Carts and collimators were specially designed to survey the equipment in PuFF facility. While the previous scoping work consisted of 32 measurements [3], the current series of assay measurements included nearly 400 measurements, with most of the increase occurring on the East Cell Line. Data analysis for the current set of measurements was conducted with greater rigor as well. MCNP was used to evaluate a variety of possible physical distributions for the Pu-238 source term and estimate cross-talk between neighboring cells. This report describes the West Cell Line hold-up measurements and subsequent data analysis.

This report is in direct support of WBS element 01.29.24.01.09.05 ("Develop Method/Design for Enhanced Characterization, Cells 3-9") as defined by the Deactivation Project Plan for the 235-F PuFF Facility [11]. Per the Deactivation Project Plan, WBS element 01.29.24.01.09.05 includes "an initial characterization of Cells 6-9 prior to decontamination and material removal activities in those cells." This

report documents one element (exterior measurements coupled with MCNP modeling) of the planned initial characterization of Cell 6-9. Other elements (e.g., in-cell measurements) of the initial characterization are planned for next FY (i.e., FY15) with results to be documented in separate, future reports.

2.0 Data Collection

On August 29th, 2013, scientists from SRNL took a series of in-situ gamma-ray measurements in the maintenance trench beneath Cells 6-9 on the west line of the PuFF facility. The detector used was a 20%-efficient, p-type HPGe detector with a 1.27 mm aluminum endcap. The detector's efficiency calibration was verified on the day of the measurements using a Cs-137 check source. A Canberra Lynx MCA was used to provide high-voltage and preamp power to the detector as well as process the detector signals. A Panasonic TOUGHBOOK tablet computer was used to run Canberra's Genie 2000 software [14], which controlled the MCA and saved the spectral data. A specialized cart was fabricated to hold the detector in a vertical orientation, aimed at the floor of the cells above. The detector, LN dewar, signal cables, Lynx MCA, and tablet computer were all wrapped in plastic to prevent Pu-238 contamination. Initial data acquisitions were attempted using a large tungsten-shot collimator, which narrowed the detector's view of the floor to a roughly 75 cm diameter circular region. The count rates obtained in this manner were unreasonably low, thus data were taken with the detector completely uncollimated. Seven fifteen-minute measurements were taken, three beneath Cell 6, two beneath Cell 7, and one beneath each of Cells 8 and 9. The major gamma-rays (99.85 keV, 152.7 keV, and 766.4 keV) of Pu-238 were clearly present in all acquired spectra except the spectrum taken under Cell 9. The gamma-ray energies found in the spectrum acquired under Cell 9 are associated with K-40 and the decay chain of Th-232, both naturally occurring radioisotopes. During all measurements, the face of the detector was located 106.7 cm beneath the floor of the cells. The location of the detector in the plane parallel to the cell floor was recorded for each measurement. A diagram showing the approximate location of each measurement in relation to the West Cell Line geometry is shown in Figure 2-1.

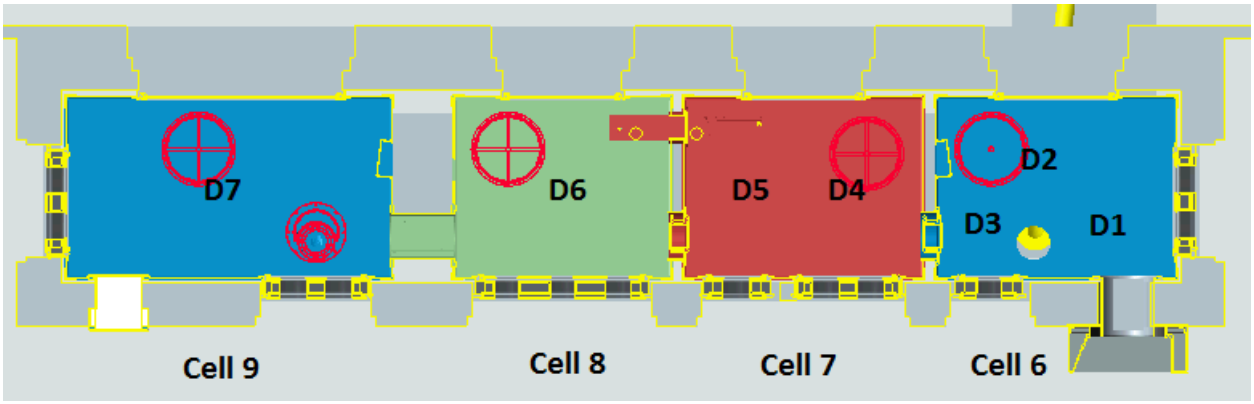

Figure 2-1: West Cell Line Geometry and Assay Locations.

On August 28th and 29th, 2014 a series of scoping measurements were performed using a well-collimated LaBr detector. Fourteen measurements were taken with the detector pointed up at the cell floors: three in each of Cells 6-8 and 5 in Cell 9. These measurements each had a view of a roughly 40 cm diameter region of the cell floors. One measurement was taken beneath the cooler in each cell. Twelve measurements were taken with the detector pointed into the cells flush to the rough center of the Lexan gloveport covers (~38 cm above the cell floors), one in each glove port. The gloveports can be seen in Figure 2-1: four in Cell 9 and three in each of Cells 6-8. These measurements were not used directly in data analysis, but were instead used as supporting evidence for likely distributions of Pu-238 in the West Cell Line. The sequence of LaBr measurements showed no indication of Pu-238 in Cells 8 or 9. The measurements indicated that in Cells 6 and 7 the Pu-238 hold-up was distributed fairly evenly through the cells, with Cell 6 containing roughly 5-10 times more material than Cell 7.

3.0 MCNP Simulations

To estimate the gamma-ray flux at the detector locations per gamma-ray emitted by Pu-238, a simulation of the west cell line of PuFF was created using the MCNP5 [2] software created by LANL. This program was used to determine the geometric solid angle of the detector relative to the source geometry as well as corrections for attenuation of the gamma-ray flux through intervening material in the cells. All simulations were run until the statistical uncertainty arising from the Monte-Carlo process was negligible.

3.1 Cell Geometry and Materials

Cells 6-9 were modeled as four box-shaped enclosures composed of 316 stainless steel with dimensions based on SRS engineering drawings [5,6]. The walls and ceilings were modeled as 3.2 mm thick and the floor was 4.76 mm thick. The interior dimensions of the cells are given in Table 3-1. There are gaps between adjacent cell walls. The width of the gaps between Cells 6 and 7 as well as Cells 7 and 8 is 11.11 cm. The width of the gap between Cells 8 and 9 is 52.71 cm. The material compositions and densities used in the simulation were taken from Reference 12. These compositions are summarized in Table 3-2. The cell floors are supported from below by a mesh pattern of 3-inch, C-channel, carbon steel girders with a linear density of 4.1 pounds per foot. Rather than include the complicated details of this mesh pattern in the simulation, the attenuation arising from the girders was included by approximating the girder geometry as a uniform, 7.62 cm layer of carbon steel with the same mass as the girders. The overall length of girders beneath each cell was estimated from engineering drawings [5,6] and used to derive the density of the girder layer for each cell. Table 3-3 contains the estimated girder lengths and effective densities used in the MCNP simulation.

Each cell contains a cooled storage container, a 55.88-cm diameter, stainless steel cylinder that extends 43.5 cm beneath the cell floor. Each cooled storage container has six interior tubes used to store Pu-238 during production. Rather than include these individual tubes in the MCNP simulation, the wall thickness of the external cylinder was modified as the sum of the actual exterior wall and the wall thickness of interior tubes, the net result being 1.4 cm. The interior of the cooled storage container was modeled as water. Each cell contains a variety of items used to produce, test, and decontaminate the iridium-clad Pu-238 spheres and pellets. Solid Waste and F-Area Engineering has compiled an inventory of the items in the cells based on engineering drawings and photographic evidence [8]. Based on this inventory, masses for the items in the cells were estimated. The items in the cells were primarily stainless steel, thus a uniform layer of stainless steel was included in the MCNP simulation with a density based on these mass estimates. Models were run with high, mid-range, and low estimates of the density of this layer. The fill height and density of this layer are found in Table 3-4.

Cell	Length (cm)	Width (cm)	Height (cm)
6	201.93	152.4	208.28
7	201.93	152.4	208.28
8	182.88	152.4	208.28
9	274.32	152.4	208.28

Table 3-1: Dimensions of Cells 6-9 used in the MCNP simulation. Length is along the north-south axis, width along the east-west axis.

Material	Density (g/cm^3)	Element	Mass or Atom* Fraction
Stainless Steel 316	7.92**	Silicon	0.010
		Chromium	0.170
		Manganese	0.020
		Iron	0.655
		Nickel	0.120
		Molybdenum	0.025
Carbon Steel	7.82**	Carbon	0.005
		Iron	0.995
Water	1.0	Hydrogen	0.666667*
		Oxygen	0.333333*
Borosilicate Fiberglass	0.02	Boron	0.040063
		Oxygen	0.539561
		Sodium	0.028191
		Aluminum	0.011644
		Silicon	0.377220
		Potassium	0.003321

Table 3-2: Material Compositions and Densities used in MCNP simulation. Elemental compositions are given by mass fraction except for those indicated by an asterisk (*) that were given by atom fraction. Densities marked with a double asterisk (**) were varied in the geometry to simulate a group of discrete items as a uniform layer of material with a lower density. Elemental compositions were taken from Reference 12.

Cell	Estimated Girder Length (ft)	MCNP Girder Density (g/cm^3)
6	35	0.278
7	40	0.318
8	35	0.307
9	50	0.293

Table 3-3: Girder Densities used in MCNP simulation. Floor support girders were simulated as a uniform layer of carbon steel 7.62 cm thick directly beneath the cell floors.

Cell	Fill Height (cm)	High Density Estimate (g/cm^3)	Middle Density Estimate (g/cm^3)	Low Density Estimate (g/cm^3)
6	45	0.135	0.095	0.056
7	30	0.053	0.039	0.026
8	30	0.080	0.057	0.034
9	30	0.088	0.058	0.028

Table 3-4: Material Fill Height and Densities used in the MCNP simulation. Material inventory within each of the cells was simulated as a uniform layer of stainless steel directly above the cell floor.

3.2 Source Distributions

The photon sources modeled in the MCNP simulation all emitted gamma-rays isotropically at three discrete energies, 99.85 keV, 152.7 keV, and 766.4 keV. A variety of source distributions were modeled to estimate the uncertainty in the overall detector efficiency arising from gamma attenuation and solid angle effects. The source distributions were applied to each cell one at a time. The following source distributions were modeled:

Floor: Photon source uniformly distributed on the floor of the cells,

Ceiling: Photon source uniformly distributed on the ceiling of the cells without the extra material layer described in Table 3-4,

Walls: Photon source uniformly distributed on the walls of the cells without the extra material layer described in Table 3-4,

Uniform: Photon source uniformly distributed throughout the volume of each cell without the extra material layer described in Table 3-4 representing an airborne distribution,

Material Layer (ML): Photon source uniformly distributed throughout the middle-density material layer described in Table 3-4,

High Material Layer (HML): Photon source uniformly distributed throughout the high-density material layer described in Table 3-4,

Low Material Layer (LML): Photon source uniformly distributed throughout the low-density material layer described in Table 3-4,

Ceiling Material Layer (CML): Photon source uniformly distributed on the ceiling of the cells with the middle-density material layer described in Table 3-4 acting as an attenuator,

Wall Material Layer (WML): Photon source uniformly distributed on the walls of the cells with the middle-density material layer described in Table 3-4 acting as an attenuator,

Coolers: Photon source uniformly distributed within the volume of the cooled storage units beneath each cell,

and **HEPA:** Photon source uniformly distributed within the HEPA filter in each cell with the middle-density material layer described in Table 3-4 acting as an attenuator.

3.3 Photon Flux at Detectors

Point detector tallies were placed in the MCNP simulation at each of the locations where measurements were performed beneath the cells. These tallies give the photon flux per source photon emitted in units of cm^{-2} at the tally location. Since the photopeaks measured by the detector only reflect photons that traveled unscattered from the source distribution to the detector, scattering was turned off in the simulation. This did not remove the effects of attenuation; rather it removes buildup calculations from the simulation, which would only serve to convolute the desired results. The photon flux was summed for all detectors beneath a particular cell (i.e. D1, D2, and D3 were summed since they were all beneath Cell 6). The photon flux resulting from source distributions in neighboring cells was included in the simulation to allow deconvolution of cross talk between cells. The photon flux on the detectors beneath the i^{th} cell per source photon arising from the j^{th} cell, ϕ_{ij}, estimated by the MCNP simulations for the various source distributions given in Section 3.2 for the 99.85 keV, 152.7 keV, and 766.4 keV photons from Pu-238 are found in Table 3-5, Table 3-6, and Table 3-7, respectively. Results for the various source distributions can be combined using weighted averages to produce results for alternate scenarios (i.e. to assume 80% of the material is on the floor, 19% is on the walls, and 1% is airborne: $\phi_{net} = 0.8\phi_{Floor} + 0.19\phi_{Walls} + 0.01\phi_{Uniform}$).

Source Distribution	ϕ_{66} (cm^{-2})	ϕ_{77} (cm^{-2})	ϕ_{88} (cm^{-2})	ϕ_{99} (cm^{-2})	ϕ_{67} (cm^{-2})	ϕ_{76} (cm^{-2})	ϕ_{86} (cm^{-2})	ϕ_{87} (cm^{-2})
Floor	7.87E-07	4.65E-07	2.97E-07	2.17E-07	9.95E-08	5.27E-08	1.38E-10	2.60E-08
Ceiling	1.95E-07	9.60E-08	6.85E-08	5.06E-08	2.94E-08	2.29E-08	5.09E-10	1.29E-08
Walls	3.09E-07	1.73E-07	1.01E-07	7.96E-08	6.02E-08	3.84E-08	5.53E-10	2.56E-08
Uniform	3.98E-07	2.22E-07	1.45E-07	1.07E-07	7.12E-08	4.48E-08	4.39E-10	3.09E-08
ML	3.14E-07	3.20E-07	1.88E-07	1.35E-07	8.56E-08	2.94E-08	1.63E-10	3.48E-08
LML	4.12E-07	3.46E-07	2.13E-07	1.61E-07	9.35E-08	3.96E-08	2.51E-10	3.82E-08
HML	2.48E-07	2.96E-07	1.66E-07	1.15E-07	7.82E-08	2.27E-08	1.19E-10	3.16E-08
CML	5.78E-08	1.20E-07	6.42E-08	4.58E-08	4.00E-08	7.09E-09	1.30E-10	1.76E-08
WML	3.52E-08	5.99E-08	3.48E-08	2.52E-08	1.81E-08	3.90E-09	2.45E-10	7.65E-09
Coolers	1.73E-08	2.07E-08	4.97E-09	9.96E-09	2.17E-09	1.30E-09	1.36E-10	6.44E-10
HEPA	3.45E-08	7.80E-08	3.48E-08	3.42E-08	3.97E-08	2.20E-09	1.95E-11	9.95E-09

Table 3-5: Photon Flux per 99.85 keV Source Photon from MCNP Simulation. The subscripts on ϕ_{ij} denote the flux on the detectors beneath the i^{th} cell from photons arising in the j^{th} cell.

Source Distribution	ϕ_{66} (cm^{-2})	ϕ_{77} (cm^{-2})	ϕ_{88} (cm^{-2})	ϕ_{99} (cm^{-2})	ϕ_{67} (cm^{-2})	ϕ_{76} (cm^{-2})	ϕ_{86} (cm^{-2})	ϕ_{87} (cm^{-2})
Floor	2.85E-06	1.80E-06	1.09E-06	8.38E-07	5.20E-07	2.74E-07	3.56E-09	1.71E-07
Ceiling	6.11E-07	3.19E-07	2.20E-07	1.61E-07	1.26E-07	8.34E-08	1.15E-08	4.42E-08
Walls	1.09E-06	6.60E-07	3.72E-07	3.03E-07	2.69E-07	1.56E-07	9.74E-09	1.06E-07
Uniform	1.33E-06	7.92E-07	4.90E-07	3.67E-07	3.09E-07	1.74E-07	8.58E-09	1.25E-07
ML	1.53E-06	1.35E-06	7.83E-07	5.92E-07	4.45E-07	1.72E-07	2.48E-09	1.75E-07
LML	1.78E-06	1.41E-06	8.38E-07	6.49E-07	4.67E-07	2.07E-07	3.38E-09	1.85E-07
HML	1.31E-06	1.30E-06	7.33E-07	5.41E-07	4.22E-07	1.44E-07	1.91E-09	1.65E-07
CML	4.41E-07	5.28E-07	2.99E-07	2.17E-07	2.13E-07	6.04E-08	5.55E-09	8.61E-08
WML	2.56E-07	2.52E-07	1.56E-07	1.13E-07	9.49E-08	3.67E-08	7.88E-09	3.35E-08
Coolers	2.89E-07	2.71E-07	9.12E-08	1.48E-07	5.51E-08	3.18E-08	2.03E-09	9.94E-09

Table 3-6: Photon Flux per 152.7 keV Source Photon from MCNP Simulation. The subscripts on ϕ_{ij} denote the flux on the detectors beneath the i^{th} cell from photons arising in the j^{th} cell.

Source Distribution	ϕ_{66} (cm^{-2})	ϕ_{77} (cm^{-2})	ϕ_{88} (cm^{-2})	ϕ_{99} (cm^{-2})	ϕ_{67} (cm^{-2})	ϕ_{76} (cm^{-2})	ϕ_{86} (cm^{-2})	ϕ_{87} (cm^{-2})
Floor	6.95E-06	4.61E-06	2.66E-06	2.15E-06	1.84E-06	9.79E-07	4.66E-08	6.96E-07
Ceiling	1.32E-06	7.29E-07	4.87E-07	3.57E-07	4.32E-07	2.80E-07	9.43E-08	1.95E-07
Walls	2.61E-06	1.67E-06	9.06E-07	7.65E-07	9.24E-07	5.34E-07	9.32E-08	4.06E-07
Uniform	3.03E-06	1.90E-06	1.13E-06	8.64E-07	9.81E-07	5.34E-07	8.38E-08	4.39E-07
ML	4.67E-06	3.67E-06	2.09E-06	1.66E-06	1.59E-06	7.11E-07	3.76E-08	6.66E-07
LML	4.96E-06	3.72E-06	2.14E-06	1.71E-06	1.62E-06	7.67E-07	4.29E-08	6.80E-07
HML	4.40E-06	3.61E-06	2.04E-06	1.60E-06	1.56E-06	6.59E-07	3.32E-08	6.51E-07
CML	1.76E-06	1.46E-06	8.50E-07	6.30E-07	7.85E-07	3.35E-07	7.59E-08	3.58E-07
WML	9.79E-07	6.71E-07	4.32E-07	3.15E-07	3.75E-07	2.23E-07	8.27E-08	1.75E-07
Coolers	3.13E-06	2.46E-06	1.03E-06	1.40E-06	9.22E-07	5.30E-07	2.38E-08	1.10E-07

Table 3-7: Photon Flux per 766.4 keV Source Photon from MCNP Simulation. The subscripts on ϕ_{ij} denote the flux on the detectors beneath the i^{th} cell from photons arising in the j^{th} cell.

4.0 Data Analysis

To calculate the mass of Pu-238 in each of Cells 6-9 the following formula was used:

$$M_{^{238}Pu} = \frac{N_{net}}{S_{^{238}Pu} \cdot BR_{\gamma} \cdot \varepsilon \cdot t} \qquad \textbf{Equation 4-1}$$

where,

N_{net} = the net count rate for the system of detectors beneath the cell in question (or the minimum detectable count rate if applicable),

$S_{^{238}Pu}$ = the specific activity of Pu-238 (6.336×10^{11} Bq/gram ± 0.1%),

BR_{γ} = the absolute branching ratio of the gamma-ray used for the analysis,

t = the assay live time (900 seconds),

ε = the detector efficiency at the energy of the gamma-ray used for the analysis

4.1 Total Counts

The major three gamma-rays emitted by Pu-238 were used for the analysis: 99.85 keV, 152.7 keV, and 766.4 keV. PeakEasy 4.51 [9] software developed by LANL was used to fit and integrate the three photopeaks in each measured spectrum. Table 4-1 contains the photopeak integrals and uncertainties for each measurement as well as the total counts measured in Cells 6 and 7.

Spectrum Name	Cell	99.85 keV Counts	152.7 keV Counts	766.4 keV Counts
D1	6	$1.880 \times 10^5 \pm 0.2\%$	$8.02 \times 10^4 \pm 0.4\%$	$1.37 \times 10^3 \pm 3\%$
D2	6	$1.350 \times 10^5 \pm 0.3\%$	$6.64 \times 10^4 \pm 0.4\%$	$1.23 \times 10^3 \pm 3\%$
D3	6	$1.035 \times 10^5 \pm 0.3\%$	$4.61 \times 10^4 \pm 0.5\%$	$8.8 \times 10^2 \pm 4\%$
Cell 6 Total	6	$4.264 \times 10^5 \pm 0.2\%$	$1.927 \times 10^5 \pm 0.2\%$	$3.48 \times 10^3 \pm 2\%$
D4	7	$4.22 \times 10^4 \pm 0.5\%$	$2.25 \times 10^4 \pm 0.7\%$	$4.6 \times 10^2 \pm 5\%$
D5	7	$3.13 \times 10^4 \pm 0.6\%$	$1.58 \times 10^4 \pm 0.9\%$	$3.2 \times 10^2 \pm 7\%$
Cell 7 Total	7	$7.35 \times 10^4 \pm 0.4\%$	$3.83 \times 10^4 \pm 0.6\%$	$7.7 \times 10^2 \pm 4\%$
D6	8	$1.16 \times 10^3 \pm 5\%$	$1.09 \times 10^3 \pm 5\%$	$83 \pm 20\%$
D7	9	N/A	N/A	N/A

Table 4-1: Counts in major Pu-238 photopeaks for each HPGe measurement. Cells 6 and 7 had multiple measurement, thus the totals for their measurements are included. There were no photopeaks associated with Pu-238 in the Cell 9 measurements.

Since the detector was uncollimated, there was cross-talk between the neighboring cells. The MCNP simulations modeled these effects by estimating the flux on the detectors beneath one cell per source photon arising in another. Let's define the following parameters (for a particular photopeak):

C_i = the total number of counts measured beneath Cell *i*,

C_{ij} = the total number of counts measured beneath Cell *i* from photons arising in Cell *j*,

and ϕ_{ij} = the flux on the detectors beneath Cell *i* per source photon arising in Cell *j*.

If Cell *j* has a substantially greater count rate than Cell *i*, then the following equation is valid:

$$C_{ii} = C_i - \frac{\phi_{ij}}{\phi_{jj}} C_j \text{.} \quad \textbf{Equation 4-2}$$

However, if there are substantial counts in Cell *i* from Cell *j* and vice versa, the following equations must be used:

$$C_{ii} = C_i - \frac{\phi_{ij}}{\phi_{jj}} C_{jj} \quad \textbf{Equation 4-3}$$

and

$$C_{jj} = C_j - \frac{\phi_{ji}}{\phi_{ii}} C_{ii} \textbf{. Equation 4-4}$$

This pair of coupled equation may be expanded into an infinite series as follows:

$$C_{ii} = \left(C_i - \frac{\phi_{ij}}{\phi_{jj}} C_j \right) \left[1 + \frac{\phi_{ij}\phi_{ji}}{\phi_{ii}\phi_{jj}} - \left(\frac{\phi_{ij}\phi_{ji}}{\phi_{ii}\phi_{jj}} \right)^2 + \left(\frac{\phi_{ij}\phi_{ji}}{\phi_{ii}\phi_{jj}} \right)^3 - \ldots \right] \quad \textbf{Equation 4-5}$$

The uncertainty in C_{ii} must be derived. It is conservative to neglect the covariance associated with the uncertainty in the ϕ_{ij} terms. For simplicity, the expansion term will be defined as:

$$E_\phi \equiv \left[1 + \frac{\phi_{ij}\phi_{ji}}{\phi_{ii}\phi_{jj}} - \left(\frac{\phi_{ij}\phi_{ji}}{\phi_{ii}\phi_{jj}} \right)^2 + \left(\frac{\phi_{ij}\phi_{ji}}{\phi_{ii}\phi_{jj}} \right)^3 - \ldots \right] \quad \textbf{Equation 4-6}$$

It is sufficient to calculate the uncertainty in the expansion to first order, thus:

$$\partial E_\phi = \left(\frac{\phi_{ij}\phi_{ji}}{\phi_{ii}\phi_{jj}} \right) \sqrt{ \left(\frac{\partial \phi_{ij}}{\phi_{ij}} \right)^2 + \left(\frac{\partial \phi_{ji}}{\phi_{ji}} \right)^2 + \left(\frac{\partial \phi_{ii}}{\phi_{ii}} \right)^2 + \left(\frac{\partial \phi_{jj}}{\phi_{jj}} \right)^2 } \quad \textbf{Equation 4-7}$$

Thus the uncertainty in C_{ii} is as follows:

$$\partial C_{ii} = \sqrt{ E_\phi^2 \left[\partial C_i^2 + \left(\frac{\phi_{ij}}{\phi_{jj}} C_j \right)^2 \left[\left(\frac{\partial \phi_{ij}}{\phi_{ij}} \right)^2 + \left(\frac{\partial \phi_{jj}}{\phi_{jj}} \right)^2 + \left(\frac{\partial C_j}{C_j} \right)^2 \right] \right] + \partial E_\phi^2 \left(C_i - \frac{\phi_{ij}}{\phi_{jj}} C_j \right)^2 } \quad \textbf{Equation 4-8}$$

The net counts in Cells 6 and 7 and their associated uncertainties were calculated from the gross counts given in Table 4-1 using Equations 4-5 through 4-8. After applying Equation 4-2 to Cell 8, it is apparent that all counts measured beneath the cell arise from Pu-238 holdup in Cells 6 and 7. Thus, MDA calculations are required for both Cells 8 and 9. To determine the minimum number of detectable counts in a photopeak the Currie formula [10] is used:

$$MDA = 2.71 + 4.65\sqrt{N_{cont}} \quad \textbf{Equation 4-9}$$

where, N_{cont} is the number of counts in the continuum at the location where the photopeak should be. To determine this quantity, PeakEasy 4.51 [9] was used to integrate the continuum in spectra D6 and D7 in a region one FWHM on either side of the central peak energy. The FWHM calibration for the detector is given by $FWHM(keV) = 0.7389 + 0.0302\sqrt{E(keV)}$. Net counts or MDAs for each of the photopeaks used in the analysis may be found in Table 4-2.

Cell	99.85 keV Counts	152.7 keV Counts	766.4 keV Counts
6	$4.16 \times 10^5 \pm 3.5\%$	$1.87 \times 10^5 \pm 5\%$	$3.3 \times 10^3 \pm 8\%$
7	$3.9 \times 10^4 \pm 14\%$	$1.8 \times 10^4 \pm 17\%$	$2.6 \times 10^2 \pm 31\%$
8	$\leq 2.3 \times 10^2$	$\leq 2.3 \times 10^2$	$\leq 6.3 \times 10^1$
9	$\leq 1.8 \times 10^2$	$\leq 1.7 \times 10^2$	$\leq 5.5 \times 10^1$

Table 4-2: Net counts for each of Cells 6-9.

4.2 Detector Efficiency

The detector efficiency for the HPGe was measured using two point sources: a Ho-166m source (IPL-1278-38) and a mixture of Eu-152, Eu-154, and Eu-155 (EZ-1480-93-10 and EZ-1480-93-9). The europium isotope blend was produced at SRNL from two liquid standards that were mixed and dried on a planchet. The sources were located 38.1 cm from the face of the detector directly on its central axis. The efficiency curve for this detector was determined using Canberra's Genie 2000 software [14] and is shown in Figure 4-1. Since the measurements taken in the west cell line of PuFF were uncollimated, photons from the cells could enter the detector at a variety of angles (no backward angles). To quantify the effect this had on the measurements, additional point source measurements were made using a Ho-166m source (IPL 482-50-1). These measurements were taken at five angles relative to the detector's central axis (0°, 22.5°, 45°, 67.5°, and 90°) at a distance of 45.72 cm from the center of the germanium crystal. The Ho-166m gamma-rays at 80.6 keV, 184.4 keV, and 752.3 keV were used to approximate the

effects to the Pu-238 gamma rays at 99.85 keV, 152.7 keV, and 766.4 keV, respectively. The variation in count rate measured over the five angles weighted by 0.683 was used as a 1σ uncertainty to account for this effect. The effect was negligible at 752.3 keV and quite strong at 80.6 keV (23%). The detector efficiency for a point source at 38.1 cm from the face of the detector and associated uncertainties arising from curve fitting, source activity, and incidence angle are found in Table 4-3**.**

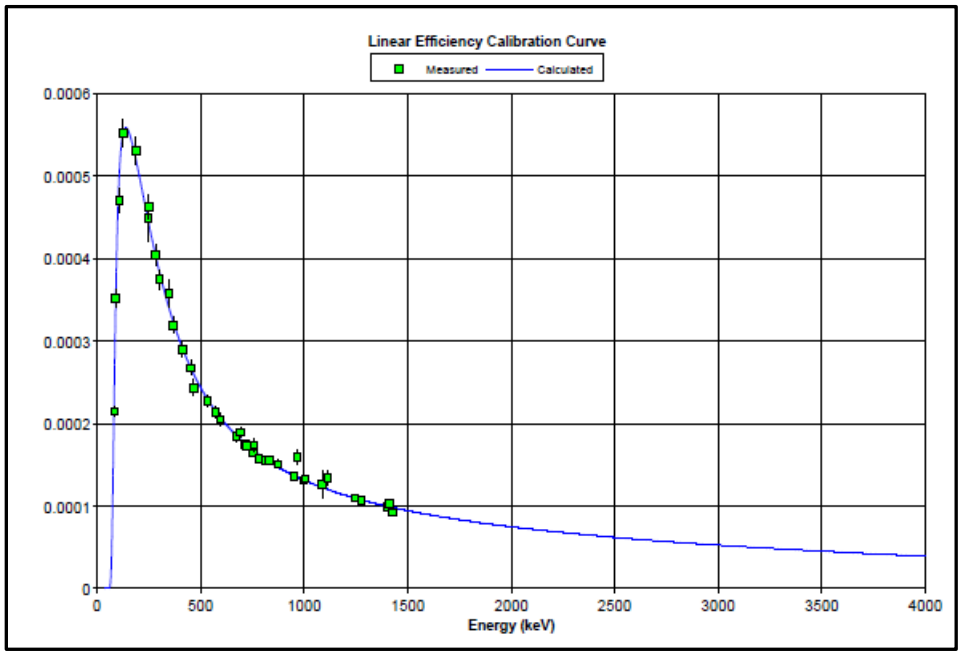

Figure 4-1: Point Source Efficiency for HPGe Detector located 38.1 cm from Ho-166m, Eu-152, Eu-154, and Eu-155 gamma-ray sources.

Energy (keV)	Efficiency	Fit Error (%)	Source Activity Error (%)	Incidence Angle Error (%)	Total Error (%)
99.85	4.30×10^{-4}	1.8	3.0	23	23
152.7	5.94×10^{-4}	1.8	3.0	3.8	5.2
766.4	1.66×10^{-4}	0.8	3.0	0	3.1

Table 4-3: Point Source Efficiencies and Associated Uncertainties

4.3 Solid Angle and Attenuation Corrections

The overall detector efficiency (ε) defined as the probability that a gamma-ray emitted by the Pu-238 is detected by the HPGe detector may be expressed as three independent parameters as follows:

$$\varepsilon = \varepsilon_0 \alpha \, \Omega \quad \textbf{Equation 4-10}$$

where, ε_0 is the energy-dependent intrinsic detector efficiency (the probability that a photon that hits the detector is counted in the photopeak), α is the energy-dependent attenuation coefficient (the fraction of photons emitted in the direction of the detector that arrive unscattered), and Ω is the average solid angle of the detector relative to the source distribution (the fraction of photons emitted by the source emitted in the direction of the detector).

The intrinsic detector efficiency is the same for the point source calibration and the detector measurements, excluding effects from the angle of incidence that are taken into account as uncertainty in the point source efficiency calculations in Section 4.2. The MCNP calculations detailed in Section 3 provide the product of the attenuation coefficient and the solid angle, which will be defined as ϕ_{MCNP}, the photon flux (cm^{-2}) at the detector face normalized per source photon (at the energy used for the analysis) from the source distributions modeled. This same parameter may be defined for the point source calibration configuration as ϕ_p, the photon flux (cm^{-2}) at the detector face normalized per source photon from a point source located 38.1 cm from the face of the detector. Thus the detector efficiency for the assay geometry is given as follows:

$$\varepsilon = \varepsilon_p \left(\frac{\phi_{MCNP}}{\phi_p} \right) \quad \textbf{Equation 4-11}.$$

Making this substitution into $M_{^{238}Pu} = \dfrac{N_{net}}{S_{^{238}Pu} \cdot BR_\gamma \cdot \varepsilon \cdot t}$ Equation 4-1, the equation used to calculate the holdup mass of Pu-238 in the cells becomes:

$$M_{^{238}Pu} = \frac{N_{net} \cdot \phi_p}{S_{^{238}Pu} \cdot BR_\gamma \cdot \varepsilon_p \cdot \phi_{MCNP} \cdot t} \quad \textbf{Equation 4-12}$$

Since attenuation is negligible for the point source calibration geometry, the parameter, ϕ_p, and its uncertainty may be calculated as follows:

$$\phi_p = \frac{1}{4\pi r^2} \quad \textbf{Equation 4-13} \quad \text{and} \quad \partial\phi_p = \frac{\partial r}{2\pi r^3} \quad \textbf{Equation 4-14}.$$

Inserting r = 38.1 ± 0.5 cm into Equations 4.10 and 4.11, ϕ_p = 5.48 × 10^{-5} cm^{-2} ± 2.6%.

After examination of the possible source distributions and the detector flux calculations from the MCNP simulation detailed in Sections 3.2 and 3.3, the values used for ϕ_{MCNP} in each of the cells was based on the average and standard deviation from the MCNP simulations based on the Floor, Material Layer, High Material Layer, Low Material Layer, and Wall Material Layer source distributions. . These values are given in Table 4-4, where $\phi_{ii} = \phi_{MCNP}$ for the i^{th} cell. The cross terms in Table 4-4, the ϕ_{ij} s, are used to determine the cross talk between neighboring cells, as described in Section 4.1. Some source configurations were modeled, but not included in the final calculation. The Uniform, Ceiling, and Ceiling Material Layer configurations were not included because it is unlikely that the majority of the Pu-238 is airborne or settled on the ceiling. The Cooler configuration was not included because the LaBr scoping measurements indicated that the Pu-238 was not in the coolers. The Wall configuration was not included because it did not include the attenuating material layer; instead the Wall Material Layer configuration was used. The HEPA configuration gave essentially identical results as the Wall Material Layer configuration. Thus averaging the five distributions mentioned above gives the effect of having twenty percent of the material in either the HEPA or settled on the walls and the remaining eighty percent of the material either settled directly on the floor or distributed on and in the various equipment remaining in the cells.

Energy (keV)	ϕ_{66} **(cm^{-2})**	ϕ_{77} **(cm^{-2})**	ϕ_{88} **(cm^{-2})**	ϕ_{99} **(cm^{-2})**	ϕ_{67} **(cm^{-2})**	ϕ_{76} **(cm^{-2})**	ϕ_{86} **(cm^{-2})**	ϕ_{87} **(cm^{-2})**
99.85	3.6E-07 ± 69%	3.0E-07 ± 44%	1.8E-07 ± 47%	1.3E-07 ± 48%	7.5E-08 ± 39%	3.0E-08 ± 55%	1.8E-10 ± 30%	2.8E-08 ± 39%
152.7	1.6E-06 ± 54%	1.2E-06 ± 42%	7.2E-07 ± 43%	5.5E-07 ± 44%	3.9E-07 ± 39%	1.6E-07 ± 47%	3.8E-09 ± 55%	1.5E-07 ± 39%
766.4	4.4E-06 ± 44%	3.2E-06 ± 41%	1.9E-06 ± 40%	1.5E-06 ± 41%	1.4E-06 ± 37%	6.7E-07 ± 37%	4.9E-08 ± 39%	5.7E-07 ± 35%

Table 4-4: Photon Flux from MCNP Calculations and Associated Uncertainties.

5.0 Assay Results

The assay mass for each cell at each of the three gamma-ray energies used in the analysis was determined using Equation 4-12. The assay masses and parameters used to calculate them for Cells 6-9 may be found in Table 5-1 through Table 5-4, respectively. Since the assay masses for Cells 8 and 9 were MDAs, no uncertainties were included in Table 5-3 or Table 5-4.

Parameter	99.85 keV Value	152.7 keV Value	766.4 keV Value
Net Count Rate	$4.16 \times 10^{5} \pm 3.5\%$	$1.87 \times 10^{5} \pm 5\%$	$3.34 \times 10^{3} \pm 8\%$
Point Source Efficiency	$4.3 \times 10^{-4} \pm 23\%$	$5.9 \times 10^{-4} \pm 5.2\%$	$1.66 \times 10^{-4} \pm 3.1\%$
Point Source Flux (cm^{-2})	$5.5 \times 10^{-5} \pm 2.6\%$	$5.5 \times 10^{-5} \pm 2.6\%$	$5.5 \times 10^{-5} \pm 2.6\%$
MCNP Flux (cm^{-2})	$3.6 \times 10^{-7} \pm 69\%$	$1.6 \times 10^{-6} \pm 54\%$	$4.4 \times 10^{-6} \pm 44\%$
Specific Activity (Bq/g)	$6.336 \times 10^{11} \pm 0.1\%$	$6.336 \times 10^{11} \pm 0.1\%$	$6.336 \times 10^{11} \pm 0.1\%$
Branching Ratio	$7.29 \times 10^{-5} \pm 1.1\%$	$9.29 \times 10^{-6} \pm 0.8\%$	$2.20 \times 10^{-7} \pm 9.1\%$
Count Time (s)	900	900	900
Mass (g)	$3.6 \pm 73\%$	$2.1 \pm 54\%$	$2.0 \pm 46\%$

Table 5-1: Assay results for Cell 6 for each of the three gamma-ray energies used in analysis along with the parameters used in the calculation. The specific activity and branching ratios for Pu-238 were taken from the National Nuclear Data Center [13].

Parameter	99.85 keV Value	152.7 keV Value	766.4 keV Value
Net Count Rate	$3.9 \times 10^{4} \pm 14\%$	$1.8 \times 10^{4} \pm 17\%$	$2.6 \times 10^{2} \pm 31\%$
Point Source Efficiency	$4.3 \times 10^{-4} \pm 23\%$	$5.9 \times 10^{-4} \pm 5.2\%$	$1.66 \times 10^{-4} \pm 3.1\%$
Point Source Flux (cm^{-2})	$5.5 \times 10^{-5} \pm 2.6\%$	$5.5 \times 10^{-5} \pm 2.6\%$	$5.5 \times 10^{-5} \pm 2.6\%$
MCNP Flux (cm^{-2})	$3.0 \times 10^{-7} \pm 44\%$	$1.2 \times 10^{-6} \pm 42\%$	$3.3 \times 10^{-6} \pm 41\%$
Specific Activity (Bq/g)	$6.336 \times 10^{11} \pm 0.1\%$	$6.336 \times 10^{11} \pm 0.1\%$	$6.336 \times 10^{11} \pm 0.1\%$
Branching Ratio	$7.29 \times 10^{-5} \pm 1.1\%$	$9.29 \times 10^{-6} \pm 0.8\%$	$2.20 \times 10^{-7} \pm 9.1\%$
Count Time (s)	900	900	900
Mass (g)	$0.40 \pm 52\%$	$0.26 \pm 46\%$	$0.21 \pm 53\%$

Table 5-2: Assay results for Cell 7 for each of the three gamma-ray energies used in analysis along with the parameters used in the calculation. The specific activity and branching ratios for Pu-238 were taken from the National Nuclear Data Center [13].

Parameter	99.85 keV Value	152.7 keV Value	766.4 keV Value
Net Count Rate	$\leq 2.3 \times 10^{2}$	$\leq 2.3 \times 10^{2}$	$\leq 6.3 \times 10^{1}$
Point Source Efficiency	4.3×10^{-4}	5.9×10^{-4}	1.66×10^{-4}
Point Source Flux (cm^{-2})	5.5×10^{-5}	5.5×10^{-5}	5.5×10^{-5}
MCNP Flux (cm^{-2})	1.8×10^{-7}	7.2×10^{-7}	1.9×10^{-6}
Specific Activity (Bq/g)	6.336×10^{11}	6.336×10^{11}	6.336×10^{11}
Branching Ratio	7.29×10^{-5}	9.29×10^{-6}	2.20×10^{-7}
Count Time (s)	900	900	900
Mass (g)	$\leq 4 \times 10^{-3}$	$\leq 5 \times 10^{-3}$	≤ 0.09

Table 5-3: Assay results for Cell 8 for each of the three gamma-ray energies used in analysis along with parameters used in the calculation. The specific activity and branching ratios for Pu-238 were taken from the National Nuclear Data Center [13].

Parameter	99.85 keV Value	152.7 keV Value	766.4 keV Value
Net Count Rate	$\leq 1.8 \times 10^{2}$	$\leq 1.7 \times 10^{2}$	$\leq 5.5 \times 10^{1}$
Point Source Efficiency	4.3×10^{-4}	5.9×10^{-4}	1.66×10^{-4}
Point Source Flux (cm^{-2})	5.5×10^{-5}	5.5×10^{-5}	5.5×10^{-5}
MCNP Flux (cm^{-2})	1.3×10^{-7}	5.3×10^{-7}	1.5×10^{-6}
Specific Activity (Bq/g)	6.336×10^{11}	6.336×10^{11}	6.336×10^{11}
Branching Ratio	7.29×10^{-5}	9.29×10^{-6}	2.20×10^{-7}
Count Time (s)	900	900	900
Mass (g)	$\leq 4 \times 10^{-3}$	$\leq 6 \times 10^{-3}$	≤ 0.1

Table 5-4: Assay results for Cell 9 for each of the three gamma-ray energies used in analysis along with parameters used in the calculation. The specific activity and branching ratios for Pu-238 were taken from the National Nuclear Data Center [13].

The assay results for each of the three energies considered are essentially completely independent measurements. The final assay result for Cells 6 and 7 were based on the weighted mean of the result for each of the three energies, where the weighting factor is based on the uncertainty of the measurements.

Thus the final assay mass and uncertainty are given by the following expressions:

$$\bar{M} = \frac{\sum_{i=1}^{3} \frac{M_{E_i}}{\partial M_{E_i}^2}}{\sum_{i=1}^{3} \frac{1}{\partial M_{E_i}^2}} \quad \textbf{Equation 5-1} \quad \text{and} \quad \partial \bar{M} = \left(\sum_{i=1}^{3} \frac{1}{\partial M_{E_i}^2} \right)^{-\frac{1}{2}} \textbf{. Equation 5-2}$$

Since the assay results for Cells 8 and 9 are MDAs, the lowest MDA for the three energies analyzed was reported. The final assay masses for Cells 6-9 from the current assay are reported in Table 5-5 along with the previous results from the 2006 scoping assay [3]. There was a 0.3σ difference between the two assays for Cell 6 and a 2.3σ difference for Cell 7 with the current results being higher in both cases. Both assays reported MDAs for Cells 8 and 9, the current results being slightly lower than the 2006 measurements. The total Pu-238 holdup measured in the West Cell Line of PuFF for the current assay is 2.4 ± 0.7 grams. This is 0.4σ higher than the 2006 scoping assay results. The accuracy of these results may be improved further with improved knowledge of the source distribution. In-cell measurements are planned for spring of 2015 that should provide this information.

Cell	Current Assay Mass (g)	2006 Scoping Assay Mass (g) [3]
6	2.2 ± 0.7 (32%)	1.78 ± 1.21 (68%)
7	0.25 ± 0.08 (30%)	0.055 ± 0.045 (82%)
8	< 0.004	< 0.00784
9	< 0.004	< 0.00911
Total West Cell Line	2.4 ± 0.7 (29%)	1.8 ± 1.2 (66%)

Table 5-5: Final Assay Results for Cells 6-9 compared to 2006 scoping assay results. Uncertainties are reported to 1σ.

6.0 References

[1] "Report of an Investigation into the Deterioration of the Plutonium Fuel Forms Fabrication Facility (PuFF) at the DOE Savannah River Site" Department of Energy – Nuclear Safety, DOE/NS-0002P, (1991)

[2] X-5 Monte-Carlo Team. "MCNP – A General N-Particle Transport Code, Version 5, Volume 1: Overview and Theory" Los Alamos National Laboratory. LA-UR-03-1987. (2003)

[3] D.W. Roberts. "FAMS Hold-Up Measurements for PuFF Process Cells" Savannah River Site. N-CLC-F-00700. (2006)

[4] R.G. Williams III, C.J. Gesh, and R.T. Pagh. "Compendium of Material Composition Data for Radiation Transport Modeling." Pacific Northwest National Laboratory. PNNL-15870, (2006)

[5] "Savannah River Plant Building 235-F Cell Line Plan Cells 6, 7, & 8 Equipment Arrangement Process" Savannah River Site, Drawing W448041, (1974)

[6] "Savannah River Plant Building 235-F Cell Line Plan Cell 9 Equipment Arrangement Process" Savannah River Site, Drawing W448888, (1974)

[7] "Basis for Interim Operation for Building 235-F." Savannah River Site, U-BIO-F-00003 Revision 0, (2013)

[8] J.C. Musall. Private Communication. (2014)

[9] B. Rooney, S. Garner, and P. Felsher. PeakEasy 4.51. Los Alamos National Laboratory. LA-CC-13-040. (2013)

[10] L.A. Currie. "Limits for Qualitative Detection and Quantitative Determination: Application to Radiochemistry." Anal. Chem. 40, 586-593 (1968)

[11] J.K Blankenship and J.C. Musall. "Deactivation Project Plan Plutonium Fuel Form Facility Building 235-F, Metallurgical Building" V-PMP-F00083, Savannah River Site, (2013)

[12] R.J. McConn, Jr., *et al.* "Compendium of Material Composition Data for Radiation Transport Modeling." PIET-43741-TM-963, PNNL-15870 Rev.1, Pacific Northwest National Laboratory, (2011)

[13] E. Brown and J.K Tuli. "Nuclear Data Sheets for A=234." Nuclear Data Sheets 108, 681 (2007)

[14] "Genie 2000 Spectroscopy Software: Operations Manual." Canberra Industries, Inc. (2012)

Appendix A. Example MCNP Input Deck

The input deck for the Material Layer source configuration is given below. The code was run using mcnp_pstudy to move the source distribution between the four cells automatically.

```
ASSAY SIMULATION FOR CELLS 6-9
C
C CCCCCCCCCCCCCCCCCCCCCCCCCCCCCCCCCCCCCCCCCCCCCCCCCCCCCCCCCCCCCCCCCCCCC
C
C SIMULATION OF CELLS 6-9 WITH Pu-238 GAMMA SOURCES (99, 153, AND
C 766 keV LINES ONLY).  VARIED SOURCE DISTRIBUTIONS AND QUANTITIES OF
C ATTENUATING MATERIALS WILL BE SIMULATED TO ESTIMATE UNCERTAININTY.
C
C GIRDERS BENEATH CELLS ARE SIMULATED AS A UNIFORM LAYER OF CARBON STEEL
C THE DENSITY OF THIS LAYER WAS ESTIMATED USING THE LENGTH OF GIRDER
C MATERIAL FOUND IN EACH CELL FROM DRAWINGS.  THE GIRDER CHANNEL STOCK
C USED WAS NOMINALLY 4.1 LBS/FT.
C
C CELL    GIRDER DENSITY (g/cm^3)
C 6       0.278
C 7       0.318
C 8       0.307
C 9       0.293
C
C COOLED STORAGE UNITS WILL BE SIMULATED BY REMOVING THE INTERIOR STORAGE
C COMPONENTS AND DOUBLING THE THICKNESS OF THE OUTER WALL (TO 1/2 INCH).
C THE COOLERS ARE FILLED WITH WATER
C
C CELLS ARE FILLED WITH STAINLESS STEEL MATERIAL UP TO 45 cm IN CELL 6
C AND 30 cm IN ALL OTHER CELLS.  DENSITY OF THIS MATERIAL IS BASED ON
C WEIGHT ESTIMATES FROM CELL INVENTORIES.
C
C MID RANGE ESTIMATES
C
C CELL    MATERIAL FILL DENSITY (g/cm^3)
C 6       0.095
C 7       0.039
C 8       0.057
C 9       0.058
C
C SOURCE UNIFORMLY DISTRIBUTED IN MATERIAL FILL (ONE CELL AT A TIME)
C
C @@@ CELL_NUM = 16 26 36 46
C
C MCNP_PSTUDY IS USED TO RUN A BATCH FOR THE FOUR CELLS (6,7,8,9)
C
C CCCCCCCCCCCCCCCCCCCCCCCCCCCCCCCCCCCCCCCCCCCCCCCCCCCCCCCCCCCCCCCCCCCCC
C
C CELL CARDS
C
C CCCCCCCCCCCCCCCCCCCCCCCCCCCCCCCCCCCCCCCCCCCCCCCCCCCCCCCCCCCCCCCCCCCCC
C
```

```
C CELL 6
C
10 0             7  -1                IMP:P=1  $ INTERIOR
11 100 -7.92    -2   1                IMP:P=1  $ WALLS
12 200 -0.278   -3                    IMP:P=1  $ GIRDERS
13 700 -1.0     -5                    IMP:P=1  $ COOLER INTERIOR
14 100 -7.92    -4   5                IMP:P=1  $ COOLER WALLS
15 0            -6                    IMP:P=1  $ CELL GAP
16 100 -0.095   -1  -7                IMP:P=1  $ MATERIAL FILL
C
C CELL 7
C
20 0             17 -11               IMP:P=1  $ INTERIOR
21 100 -7.92    -12  11               IMP:P=1  $ WALLS
22 200 -0.318   -13                   IMP:P=1  $ GIRDERS
23 700 -1.0     -15                   IMP:P=1  $ COOLER INTERIOR
24 100 -7.92    -14  15               IMP:P=1  $ COOLER WALLS
25 0            -16                   IMP:P=1  $ CELL GAP
26 100 -0.039   -11 -17               IMP:P=1  $ MATERIAL FILL
C
C CELL 8
C
30 0             27 -21               IMP:P=1  $ INTERIOR
31 100 -7.92    -22  21               IMP:P=1  $ WALLS
32 200 -0.307   -23                   IMP:P=1  $ GIRDERS
33 700 -1.0     -25                   IMP:P=1  $ COOLER INTERIOR
34 100 -7.92    -24  25               IMP:P=1  $ COOLER WALLS
35 0            -26                   IMP:P=1  $ CELL GAP
36 100 -0.057   -21 -27               IMP:P=1  $ MATERIAL FILL
C
C CELL 9
C
40 0             37 -31               IMP:P=1  $ INTERIOR
41 100 -7.92    -32  31               IMP:P=1  $ WALLS
42 200 -0.293   -33                   IMP:P=1  $ GIRDERS
43 700 -1.0     -35                   IMP:P=1  $ COOLER INTERIOR
44 100 -7.92    -34  35               IMP:P=1  $ COOLER WALLS
46 100 -0.058   -31 -37               IMP:P=1  $ MATERIAL FILL
C
88 0            -99 88 4 14 24 34     IMP:P=1  $ SURROUNDINGS
99 0             99                   IMP:P=0  $ THE GRAVEYARD

C CCCCCCCCCCCCCCCCCCCCCCCCCCCCCCCCCCCCCCCCCCCCCCCCCCCCCCCCCCCCCCCCCCCCCCCCCCC
C
C SURFACE CARDS
C
C CCCCCCCCCCCCCCCCCCCCCCCCCCCCCCCCCCCCCCCCCCCCCCCCCCCCCCCCCCCCCCCCCCCCCCCCCCC
C
C CELL 6
C
1   RPP     0.  201.93    0.   152.4      0.  208.28     $ INTERIOR
2   RPP -0.32   202.25 -0.32   152.72 -0.476  208.6      $ EXTERIOR
3   RPP -0.32   202.25 -0.32   152.72 -8.096 -0.476      $ GIRDERS
4   RCC  157.16  59.65 -8.096  0. 0.  -35.72  27.94      $ COOLER EXT
5   RCC  157.16  59.65 -8.096  0. 0.  -34.32  26.54      $ COOLER INT
6   RPP  202.25 213.36 -0.32   152.72 -8.096  208.6      $ CELL GAP
7   PZ   45                                              $ MATERIAL FILL
```

```
C
C CELL 7
C
11  RPP  213.68 415.61    0.   152.4      0.  208.28     $ INTERIOR
12  RPP  213.36 415.93 -0.32   152.72 -0.476  208.6      $ EXTERIOR
13  RPP  213.36 415.93 -0.32   152.72 -8.096 -0.476      $ GIRDERS
14  RCC  261.62  59.65 -8.096  0. 0.  -35.72  27.94      $ COOLER EXT
15  RCC  261.62  59.65 -8.096  0. 0.  -34.32  26.54      $ COOLER INT
16  RPP  415.93 427.04 -0.32   152.72 -8.096  208.6      $ CELL GAP
17  PZ   30                                              $ MATERIAL FILL
C
C CELL 8
C
21  RPP  427.36 610.24     0.  152.4      0.  208.28     $ INTERIOR
22  RPP  427.04 610.55 -0.32   152.72 -0.476  208.6      $ EXTERIOR
23  RPP  427.04 610.55 -0.32   152.72 -8.096 -0.476      $ GIRDERS
24  RCC  570.87  59.65 -8.096  0. 0.  -35.72  27.94      $ COOLER EXT
25  RCC  570.87  59.65 -8.096  0. 0.  -34.32  26.54      $ COOLER INT
26  RPP  610.55 663.26 -0.32   152.72 -8.096  208.6      $ CELL GAP
27  PZ   30                                              $ MATERIAL FILL
C
C CELL 9
C
31  RPP  663.58 937.90    0.   152.4      0.  208.28     $ INTERIOR
32  RPP  663.26 938.21 -0.32   152.72 -0.476  208.6      $ EXTERIOR
33  RPP  663.26 938.21 -0.32   152.72 -8.096 -0.476      $ GIRDERS
34  RCC  827.72  59.65 -8.096  0. 0.  -35.72  27.94      $ COOLER EXT
35  RCC  827.72  59.65 -8.096  0. 0.  -34.32  26.54      $ COOLER INT
37  PZ   30                                              $ MATERIAL FILL
C
88  RPP -0.32   938.21 -0.32   152.72 -8.096  208.6      $ ALL CELLS
99  RPP -100.   1000.  -100.   200.   -150.   300.       $ GRAVEYARD FENCE

C CCCCCCCCCCCCCCCCCCCCCCCCCCCCCCCCCCCCCCCCCCCCCCCCCCCCCCCCCCCCCCCCCCCCC
C
C DATA CARDS
C
C CCCCCCCCCCCCCCCCCCCCCCCCCCCCCCCCCCCCCCCCCCCCCCCCCCCCCCCCCCCCCCCCCCCCC
C
MODE P       $ TRANSPORT NEUTRONS AND PHOTONS
NPS  1E8     $ 10 MILLION SOURCE PHOTONS
NOTRN        $ ONLY DIRECT CONTRIBUTIONS TO POINT DETECTOR TALLIES
PRINT 10 30 40 50 110 140
C
C CCCCCCCCCCCCCCCCCCCCCCCCCCCCCCCCCCCCCCCCCCCCCCCCCCCCCCCCCCCCCCCCCCCCC
C
C MATERIAL CARDS
C
C CCCCCCCCCCCCCCCCCCCCCCCCCCCCCCCCCCCCCCCCCCCCCCCCCCCCCCCCCCCCCCCCCCCCC
C
C STAINLESS STEEL 316, DENSITY = 7.92 g/cm^3
C
M100      14000   -0.010       $ Si
          24000   -0.170       $ Cr
          25000   -0.020       $ Mn
          26000   -0.655       $ Fe
          28000   -0.120       $ Ni
```

```
          42000   -0.025       $ Mo
C
C CARBON STEEL, DENSITY = 7.82 g/cc
C
M200       6000   -0.005       $ C
          26000   -0.995       $ Fe
C
C PORTLAND CEMENT, DENSITY = 2.3 g/cm^3
C
M300       1001   -0.010000    $ H
           6000   -0.001000    $ C
           8000   -0.529107    $ O
          11000   -0.016000    $ Na
          12000   -0.002000    $ Mg
          13000   -0.033872    $ Al
          14000   -0.337021    $ N
          19000   -0.013000    $ K
          20000   -0.044000    $ Ca
          26000   -0.014000    $ Fe
C
C LEAD, DENSITY = 11.34 g/cm^3
C
C M400      82000    1.0         $ Pb
C
C ALUMINUM, DENSITY = 2.7 g/cm^3
C
C M500      13000    1.0         $ Al
C
C GERMANIUM, DENSITY = 5.323 g/cm^3
C
C M600      32000    1.0         $ Ge
C
C WATER, DENSITY - 1.0 g/cm^3
C
M700       1001    0.666667    $ H
          16000    0.333333    $ O
C
C CCCCCCCCCCCCCCCCCCCCCCCCCCCCCCCCCCCCCCCCCCCCCCCCCCCCCCCCCCCCCCCCCCCCCCCC
C
C SOURCE CARDS
C
C CCCCCCCCCCCCCCCCCCCCCCCCCCCCCCCCCCCCCCCCCCCCCCCCCCCCCCCCCCCCCCCCCCCCCCCC
C
C
SDEF  PAR=P              $ PHOTON SOURCE
      ERG=D1             $ ENERGY GIVEN BY DISTRIBUTION 1
      X=D2               $ SOURCE DISTRIBUTION IN X
      Y=D3               $ SOURCE DISTIRBUTION IN Y
      Z=D4               $ SOURCE DISTIRBUTION IN Z
      CEL = CELL_NUM     $ VARIABLE CELL NUMBER
      EFF=0.001          $ SAMPLING EFFICIENCY THRESHOLD
C
C ENERGY DISTRIBUTION (DISCRETE LINES)
C
SI1 L  0.099853
       0.152720
       0.76639
```

```
C
C ENERGY DISTRIBUTION PROBABILITIES (UNNORMALIZED)
C
SP1    1.
       1.
       1.
C
C SOURCE DISTRIBUTION IN X - UNIFORM OVER EXTENT OF CELLS
C
SI2 H -0.1  938.0
SP2    0.     1.
C
C SOURCE DISTRIBUTION IN Y - UNIFORM OVER EXTENT OF CELLS
C
SI3 H -0.1  152.5
SP3    0.     1.
C
C SOURCE DISTRIBUTION IN Z - UNIFORM OVER EXTENT OF CELLS
C
SI4 H -0.1   45.1
SP4    0.     1.
C
C CCCCCCCCCCCCCCCCCCCCCCCCCCCCCCCCCCCCCCCCCCCCCCCCCCCCCCCCCCCCCCCCCCCCCCCCC
C
C TALLY CARDS
C
C CCCCCCCCCCCCCCCCCCCCCCCCCCCCCCCCCCCCCCCCCCCCCCCCCCCCCCCCCCCCCCCCCCCCCCCCC
C
F5:P  83.50   100.65  -107.16  0.
      116.52  62.55   -107.16  0.
      174.31  107.0   -107.16  0.
      271.78  76.52   -107.16  0.
      354.97  76.52   -107.16  0.
      518.80  76.52   -107.16  0.
      790.26  76.52   -107.16  0.
C
FC5  PHOTON FLUX AT ASSAY POSITIONS
C
E5 0. 0.099 0.1 0.152 0.153 0.766 0.767
```

Distribution:

A.H. Couture (707-7F)
D.P. Diprete (773-41A)
R.S. Lee (773-41A)
J.C. Musall (707-7F)
E.T. Sadowski (773-A)
R.H. Young (707-7F)
D.L Beeler (707-7F)
Records Administration (EDWS)